Chapter 1

Introduction

"I don't want to believe, I want to know" - Carl Sagan

1.1 X-ray astronomy: an introduction

High energy emission from cosmic sources involve extremes of conditions like high temperature, immense density, strong gravity, high magnetic field, highly relativistic motion etc. that are unattainable on Earth. These high energy emission include radiation in X-rays and γ rays.

X-rays are a part of the electromagnetic spectrum with energies ranging from 0.1 keV-100 keV. The serendipitous discovery of X-rays by German physicist W. C. Roentgen in 1895 has been one of the most important discoveries of all times. Due to the property of X-rays to pass through flesh and bones differentially, the usefulness of X-rays in medical sciences was immediately recognized. However, the discovery of X-rays from the first astronomical source had to wait, since the technology for carrying out

research from above the atmosphere where X-rays are detected were available only after World War II. It was only in the late 1950s that the U.S Naval Research Laboratory (NRL), using V2 rockets, discovered the corona of Sun as a powerful source of X-rays. The power emitted in X-rays was however found to be a millionth times less than the total luminosity in the entire electromagnetic band. This made astronomers lose interest in the search for other X-ray sources as they believed that other source of X-rays farther away from the Sun would be much dimmer in X-rays. On the other hand, experimental results from high energy cosmic rays indicated the presence of some celestial objects which produced high energy cosmic rays in processes which further could also produce X-rays and γ rays [10, 11].

Even with such uncertainty, astronomers aimed at developing more sensitive instruments to detect X-rays from other sources. The next successful mission was a group at American Science and Engineering led by Riccardo Giacconi in June 1962. This group was searching for X-rays from Moon which they failed to detect. Instead, they discovered the existence of a powerful X-ray source, which was later named Sco X-1 in constellation Scorpious [12]. Around four months later, evidence were found for detection of two weaker sources [13], one of which NRL confirmed as the Crab Nebula - a young supernova remnant in our Galaxy [14]. After this, astronomers enthusiastically explored small areas of sky with rockets and balloons. It was *SAS*-1 (Small Astronomy Satellite 1) launched by NASA in December 1970 from Kenya that made the first all sky survey in X-rays. This first Earth orbiting mission dedicated to X-ray astronomy was later renamed *Uhuru* [15]. In slightly more than two years, about 400 X-ray sources were discovered by *Uhuru* which included accreting binaries, supernova

Table 1: Various X-Ray missions

Space Observatory	Energy Range	Mission lifetime
HEAO-1 [17]	0.2-60 keV	1977-79
HEAO-2 (*Einstein*) [18]	1-20 keV	1978-81
UHURU[15]	2-20 keV	1970-73
EXOSAT [19]	0.05-50 keV	1983-87
Ginga [20]	2-37 keV	1987-91
CGRO [21]	30 keV to 30 GeV	1991-2000
ASCA [22]	0.5-10 keV	1992-2000
ROSAT [23]	0.1-2.4 keV	1990-1999
RXTE [24]	2-100 keV	1996-2012
Beppo-SAX [25]	0.1-100 keV	1997-2003
Chandra [26]	0.1-10 keV	1999-present
XMM-Newton [27]	0.1-12 keV	2000-present
INTEGRAL [28]	15 KeV-10 MeV	2002-present
Swift [29]	0.2-150 keV	2004-present
Suzaku [30]	0.5-150 keV	2006-2015
FERMI [31]	8 keV-1 TeV	2008-present
*Nu*STAR [32]	3-79 keV	2013-present
ASTROSAT [33]	0.3-150 keV	2015-present

remnants, Seyfert galaxies and clusters of galaxies [16]. Since then, a number of space missions dedicated specifically to X-ray astronomy have been launched. The period of operation of some of the most successful missions along with the energy range in which they operated are tabulated as in Table 1.

The data accquired from these space observatories helped tremendously in enhancing our understanding of the X-ray Universe, especially accreting X-ray binaries. In this thesis, we mostly discuss the broadband spectral characteristics of High Mass X-ray Binaries (HMXBs) using *Suzaku* archived data. We also discuss the evolution of pulse profile studies of isolated pulsars with *RXTE*-PCA.

1.2 X-ray binaries-XRBs

X-ray binaries (XRBs) are a system of two stars gravitationally bound to each other which rotate about a common centre of mass. One of them is a compact object which could be a white dwarf, a neutron star or a black hole and the other is a massive companion star. Based on the mass of the companion star, X-ray binaries are classified either as High Mass X-ray Binaries (HMXBs) -when the companion mass is $\geq 10\ M_{\odot}$ or Low Mass X-ray Binaries (LMXBs)- when the companion mass is $< 2\ M_{\odot}$. A third class of X-ray binaries called the Intermediate X-ray binaries have companion masses in between the above mentioned two classes, but are extremely rare. In this thesis, we discuss the observational properties of HMXBs.

1.2.1 Accretion-what is it?

There are four kinds of forces in nature viz., Strong, Electromagnetic, Weak and the Gravitational forces. In scales of everyday world that we live in, gravity is the weakest of all forces. Of course, the General Theory of Relativity does not regard gravity as a 'force', but rather as a curvature of space-time itself. Whatever way we choose to call gravity, what is always true is that the more massive objects are, more is the gravitational attraction between them (curvature of space time is more).

Ironically, this 'weakest force' now powers the most energetic of phenomenon by what we call accretion in astrophysics. Accretion is the inflow of matter from a companion star to a massive object. The inflow takes place because of the gravitational pull of the massive, often compact object. On doing so, the gravitational potential energy of the inflowing matter converts into high energy radiation. To get an order of magnitude

estimate, let us perform a very simple calculation as follows: Assume a particle of mass m falling from a large distance to the compact object of radius R and mass M_1. At infinity, it's kinetic energy is equal to zero. As it approaches the neutron star (NS), it's kinetic energy increases because of the influence of gravitational pull of the NS, while it's potential energy decreases. Near the surface of the neutron star we have,

$$\frac{1}{2}mv^2 = \frac{GM_1m}{R} \tag{1.1}$$

where v is the free-fall velocity of the particle at R.

Assuming that all of its kinetic energy is converted into gravitational potential energy, the accretion luminosity L_{acc} (the rate of emission of radiation) becomes :

$$L_{acc} = \frac{1}{2}\dot{M}v^2 = \frac{GM_1\dot{M}}{R}$$

where $\dot{M}$ is the accreted mass (dot represents time derivative).

Of course, we know that all of the kinetic energy is not converted into radiation. Some energy may get used in spinning up the compact star (rotational kinetic energy) or may get direted into jets. The efficiency η (=Output energy/Input energy) can be calculated as:

$$\dot{\eta} = \frac{L_{acc}}{\dot{M}c^2} \tag{1.2}$$

For a typical neutron star of mass 1 $M_\odot$ and radius 10 km, we get $\eta \sim 0.15$.

We can place a limit on the maximum matter that can be accreted by using the concept of Eddington luminosity (L_{Edd}). It is defined as the maximum luminosity that a stellar object can have, when the radiation pressure that acts outward on

the electrons balances the gravitational pull on the nuclei of the infalling material. Assume matter to be composed of only ionized hydrogen. Consequently, the force of radiation can be considered to be acting only on electrons through Thomson scattering (since the scattering cross-section of photons is a factor of $(m_e/m_p)^2$ smaller, where m_e, m_p are electron and proton masses respectively). For a pair of proton and electron in the vicinity of the neutron star, we can write

$$\frac{GM_1 m_p}{R^2} = \frac{L_{Edd}\sigma_e}{4\pi R^2 c} \tag{1.3}$$

where σ_e ($= 6.6 \times 10^{-25}\text{cm}^{-2}$) is the Thomson scattering cross section for electrons. Hence,

$$L_{Edd} = \frac{4\pi G M_1 m_p c}{\sigma_e} = 1.3 \times 10^{38}(M_1/M_\odot)\text{ergs}^{-1}$$

To obtain the limiting case of mass transfer, we simply equate the accretion luminosity to the Eddington luminosity and obtain:

$$\dot{M} = \frac{4\pi R m_p c}{\sigma_e} = 1.5 \times 10^{-8}(R/10^6)M_\odot\text{yr}^{-1}$$

It should be noted that this calculation gives only an order-of-magnitude estimation based on naive assumptions. It becomes necessary also to mention here that the above is valid for persistent emissions. For transient processes like, in the case of supernova or X-ray bursts, the luminosity greatly exceeds L_{Edd} . These cases, however, will not be discussed in this thesis.

The importance of understanding of accretion lies in the fact that a large fraction of the stars are in a binary system at some point in their lifetime. In such cases, their

evolution then greatly depends on the mass transfer. Also, the fact that accretion being very efficient, is an important process for radiation (like in quasars) and outflow in astrophysics.

1.3 Accretion mechanism

There are three ways in which accretion can proceed in a binary system *viz.,*

- Roche lobe overflow,
- Stellar wind accretion,
- Accretion from Be stars

1.3.1 Roche lobe overflow

During the course of evolution of the binary system, the binary separation may decrease - because of orbital momentum loss from the system caused by stellar wind mass loss or gravitational radiation - or the companion star may increase in size such that it reaches the point where the gravitational pull of the compact object is sufficient to shred off the outer layers of the companion star. Matter then flows via an accretion disc onto the compact object. Consider the masses of two stars as M_1 and M_2. For the purpose of understanding the issue, we generally consider a test particle under the gravitational potential influence of these two stars. We consider the two stars in question to be so massive that the test particle has no influence on their motion. The orbits of these two stars are assumed to be circular, a reasonable assumption, given the fact that tidal effects circularize the originally eccentric orbits

on timescales before the mass transfer begins. In closed binary systems, each star is affected by it's own as well as the gravitational force of the other star. The effective gravitational potential (also called the Roche potential) is determined by the mass of each star as well as centrifugal force due to the motion of two stars around each other. Hence, in a frame co-rotating with the binary system, the Roche potential ϕ can be written as:

$$\phi(r) = -\frac{GM_1}{|r - r_1|} - \frac{GM_2}{|r - r_2|} - \omega^2 r^2 \tag{1.4}$$

where r_1 , r_2 are the position vectors of the centres of the two stars, r is the distance to the common rotational axis of the binary system and ω is orbital angular velocity of the system with reference to an inertial frame [1]. This potential has five points called the 'Lagrangian' points where the gradient of the effective potential is zero. They are denoted as L_1, L_2, L_3, L_4, L_5 in Figure 1.1. As can be seen from Figure 1.1, L_1, L_2 and L_3 lie along the same line joining the centres of two stars. As we approach the two stars, the equipotential surfaces are practically spherical while farther away, they are distorted. This can be explained by considering the fact that closer to the two stars, it is the gravitational potential of each star that dominates and hence the equipotential surfaces are spherical, while farther away from the star, there are tidal effects that come into play which tend to ellongate the surface along the companion star along with centrifugal forces that flatten them. Hence the net result is a distorted surface.

The mass transfer takes place via the inner Lagrangian point L_1. The infalling matter has high specific angular momentum J and hence it cannot accrete directly into the NS. Instead it will form a disc around the neutron star, which is called the

accretion disc. The particles circle in quasi-Keplarian orbits in these accretion discs and spiral inwards by transferring angular momentum by viscous dissipation effects. The formation of disc requires the obvious condition that the circularization radius R_{cir}, given by equation 1.5 (which is the radius where the specific angular momentum of the accreted material is the same as that in a circular orbit around the compact object) is greater than the size of the compact object.

$$R_{cir} = \frac{J^2}{GM_1} \tag{1.5}$$

For a typical LMXB, $R_{cir} \geq 3.5 \times 10^9 P_{hr}^{2/3}$ cm [1], which obviously make it greater than the size of a NS. Observationally too, disc formation is seen more in LMXBs. A disc may not form in cases where the compact objects where magnetic field affects the accretion process. This is the case in some HMXBs which we discuss next.

1.3.2 Stellar wind accretion

Besides disc accretion, there is another type of accretion which is the stellar wind accretion [34, 35] relevant for systems containing an early type OB stars (luminosity class I) and systems that have Be stars (luminosity class between III-V) as their companion. Accretion in these systems can be described with the Bondi-Hoyle accretion theory [36]. Assuming that the companion star loses mass in the form of a steady, homogeneous and spherically symmetric wind, the mass loss rate is given by:

$$\dot{M} = 4\pi r^2 \rho(r) v_w \tag{1.6}$$

where v_w and ρ are the stellar wind velocity and the mass density at a distance r from the companion star. The NS captures only a fraction of the emitted wind. Those

particles in the wind that pass so close to the neutron star that the gravitational potential energy in the field of the NS exceeds the kinetic energy of the particle will be accreted by the neutron star. Accretion takes place from a roughly cylindrical volume with a radius r_{acc} where r_{acc} is called the accretion radius and is defined as the maximum radial distance at which the gravitational field of the NS (of mass M_1) affect the out-flowing stellar wind, directing the material towards itself. The accretion radius is given by,

$$r_{acc} = \frac{2GM_1}{v_{rel}^2} \tag{1.7}$$

where $v_{rel}(= {v_n}^2 + {v_w}^2)^{1/2}$ is relative wind velocity, v_n is the orbital velocity of the NS about it's companion and v_w is the wind velocity.

Since the wind velocity is highly supersonic, a bow shock is formed in front of the NS as is shown in Figure 1.2. In these cases, matter accreted from the companion star very rarely form an accretion disc. If the neutron star were not orbiting the companion star, then the total angular momentum of the accreted matter would be zero by symmetry. However, this is not the case and the orbital motion of neutron star also means that the whole accretion cylinder rotates about the companion. This would make the specific angular momentum, J of the accreted material similar to that of a flat circular disc of radius r_{acc} rotating about a diameter which is given by:

$$J = \frac{1}{4} r_{acc}^2 \omega \tag{1.8}$$

In these systems, the circularization radius can be written as:

$$R_{cir} = \frac{G^3 M_1^3 \omega^3}{v_w^8} \tag{1.9}$$

In case of stellar wind accretion, we are limited by a lot of uncertainites. Firstly, we still do not have much information about the wind law. If we write $v_w^2 = \lambda(r) v_{esc}$ where $\lambda(r) \sim 1$. The uncertainty in $\lambda(r)$ by a small factor can shoot the calculation of R_{cir} way off by a huge factor since v_w varies by a power of 8 in Equation 1.9 (and hence $\lambda(r)$ raised to the power of 4). Next comes the uncertainty in determining the accretion radius r_{acc}. Nonetheless, to get a typical value, we can consider $\lambda \sim 1$ and $M_1 = 10$ $M_\odot$which leads to $R_{cir} = 1.3 \times 10^6 (10)^{1/3} (\frac{P_{orb}}{10d})^{2/3}$ cm. A typical neutron star has radius of 10^6 cm. Hence, matter coming from the companion star can accrete radially onto the neutron star. Discs may form in the case of stellar wind accretion in HMXBs, but they are smaller in size as compared to LMXBs. Depending on the companion star mass and type, we shall discuss the two separate cases as below:

Stellar wind accretion in supergiants:

These are persistant systems having an orbital period of $\sim P_{orb} \leqslant 10$ days and nearly circular orbits with eccentricity, e ≤ 0.1 [2]. These kind of companion stars have large mass loss rates of $\sim 10^{-6}$ $M_\odot$ yr^{-1} and are hence luminous, $L_X \leq 10^{37}$ erg s^{-1}. These are persistently accreting systems like Vela X-1, LMC X-4, and OAO 1657-415, to name a few.

Stellar wind accretion from Be stars:

The second group are HMXBs that comprise of transient sources that have Be stars (luminosity class between III-V) as their companion. Be stars are 'A non-supergiant B star whose spectrum has, or had at some time, one or more Balmer lines in emission'

[37]. The objects in these systems are in a wide orbit ($P_{orb} > 10$ d) and moderate eccentricity ($0.2 \leq e \leq 0.5$) as depicted in Figure 1.3 [2]. The larger companion stars undergo irregular equatorial mass ejection which produce a rotating ring of gas around it. This gives rise to hydrogen lines in the optical spectrum. The NS during passing through the circumstellar disc once every orbit accretes from this circumstellar disc around the companion star which leads to X-ray outbursts [38].

1.4 Accretion onto high magnetic field neutron stars

In addition to accretion mechanisms in different class of X-ray binaries discussed so far, we also need to consider the effect of magnetic field of the NS on the accretion flow. The magnetic field in the case of LMXBs are in the range $10^9 - 10^{11}$ G while for HMXBs, they are within the range of $10^{11} - 10^{13}$ G. Such high magnetic fields, especially the latter affect the dynamics of accretion. The radius where the ram pressure of the accreting matter is equal to the magnetic pressure is called the Alfven radius r_A. Or,

$$\frac{4\pi}{\mu_0}\frac{B(r)^2}{8\pi} = \rho v_{in}(r)^2 \tag{1.10}$$

where B and v_{in} are the magnetic field of the NS and the velocity of infalling matter at distance r from it's surface. Assuming a dipole magnetic, at Alfven radius, and since,

$$\rho = \frac{\dot{M}}{4\pi r^2 v} \tag{1.11}$$

and using Equation 1.1, we can write:

$$\frac{4\pi\mu^2}{\mu_0 8\pi {r_A}^6} = \frac{(2GM_1)^{1/2}\dot{M}}{4\pi {r_A}^{5/2}} \tag{1.12}$$

where μ is the magnetic moment. This is also called the magnetospheric radius (magnetosphere being the volume where the dynamical properties of the infalling flow is strongly affected by the magnetic field). Once matter reaches r_A, accretion onto the NS can take place only if the centrifugal force, due to the rotational velocity of the NS magnetosphere, is smaller than the gravitational force. This happens when $r_A < r_{corr}$, where r_{corr} is called the corrotation radius where,

$$r_{corr} = \frac{GM_1}{\omega^2}^{1/2} \tag{1.13}$$

Accretion is thus characterized by accretion radius, r_{acc}; magnetospheric or Alfven radius, r_A and corrotation radius, r_{corr}). In the next paragraph, we discuss different regimes that can occur depending on their relative magnitudes.

Case 1: $r_{acc} > r_A$ & $r_{corr} > r_A$: For the 'infalling' matter to be accreted onto the neutron star, we should have, at the magnetospheric radius, the Keplerian velocity of the accreting matter be greater than the velocity of the rotating magnetosphere of the neutron star. This can be fulfilled when the magnetospheric or the Alfven radius r_A, is smaller than the corrotation radius r_{corr}. In such a situation, the matter flows from r_{acc} to r_A where it is channelled along the magnetic lines of force. Matter then falls onto the poles of the neutron star where it is stopped by radiative shock or Coulomb interactions, depending on $\dot{M}$. This accumulation of matter on the neutron star poles lead to the formation of the cylindrical accretion column which radiate in X-rays. Case 2: $r_{acc} > r_A > r_{corr}$: In this case, the infalling matter is stopped at

r_A, where it loses angular momentum because of its interaction there. Since the layer closer to the compact object rotate faster than at r_A, centrifugal inhibition of accretion occur. Some or all matter maybe ejected beyond r_{acc} by propeller mechanism. Case 3: Besides the two cases mentioned above, there is another possibility that may take place for HMXBs of magnetic fields of 10^{14-15} G when $r_A > r_{acc}$: For $r_{corr} > r_{acc}$, then matter from the companion forms a shock and halts close to r_A and cannot proceed inward. The interaction between matter and the neutron star surface at r_A thus results in the loss of rotational energy and hence neutron star spins down. This is the Super-Keplerian Magnetic Inhibition. When $r_A < r_{corr}$, it is the Sub-Keplerian Magnetic Inhibition Regime and matter can now get through the neutron star magnetosphere. We do not present the detailed theory here which has been thoroughly discussed by other authors [39].

1.5 Production of X-rays

X-rays are classified either as continuous and characteristic. We discuss them briefly below:

1.5.1 Continuous X-rays

Continuous X-rays are produced either in thermal or non-thermal processes.

Thermal

- Black body emission: It is well known that any body that has temperature greater than absolute zero emit electromagnetic radiation characterized by their

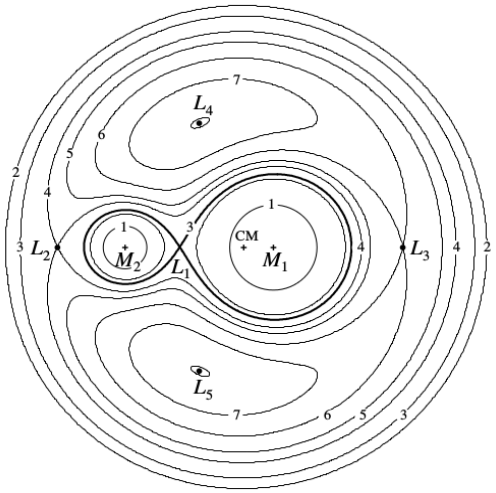

Figure 1.1: Illustrating the equipotential surfaces for a binary system with $M_2/M_1 = 0.25$. CM denotes the centre of mass, Lagrange points are marked as (L_1)-(L_5). The equipotentials are labelled by the numbers 1-7 in order of increasing $\phi(r)$. The inner Lagrange point L_1 between the two Roche lobes allow for passage of matter. Figure courtesy: [1].

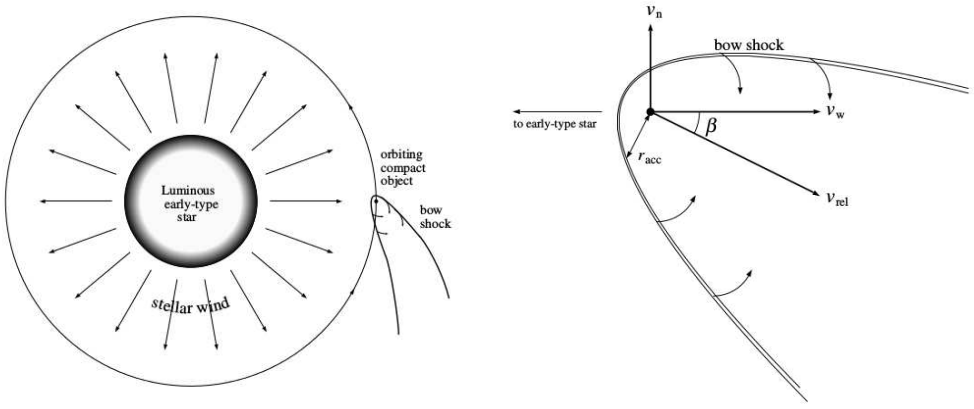

Figure 1.2: Left: Schematic representation of stellar wind accretion. Right: Illustrating the bow shock formation in stellar wind accretion. Figures courtesy: [1]

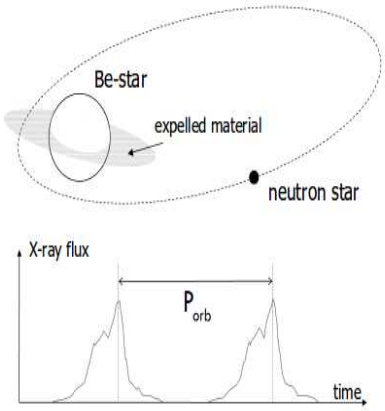

Figure 1.3: An illustration of Be stars. Figure courtesy: [2].

temperature. Likewise stars also do so. In case of neutron stars, if the surface temperature is 10^6 K or higher, it will emit blackbody radiation with photons in the X-ray regime.

- Bremsstrahlung: For temperatures around 10^6 K, the particles are ionized and in thermal equilibrium. The acceleration of an electron when it passes close to a positive ion causes it to radiate electromagnetic energy. This is called 'bremsstrahlung' (braking radiation). This component is seen when the optical depth of matter around the neutron star is low. Radiation from such electron-ion collision has a characteristic shape determined only by the temperature. This is thermal bremsstrahlung. For temperatures above 1 million degrees K, the photons emitted are in X-rays.

Non-thermal

- Synchrotron: In the presence of magnetic field, a moving electron will change

direction because the field exerts a force perpendicular to the direction of motion. Due to the acceleration of electrons this way, it emits electromagnetic energy. This is called 'magnetic bremsstrahlung' or synchrotron radiation. For relativistic speeds of electron, the radiation is compressed into small range of angles centering the instantaneous velocity. One example where synchrotron emission is seen is the radio emission from shell-like supernova remnants like Crab nebula or base of quasar jets.

- Inverse Comptonization: This involves the scattering of low energy photons to high energies by electrons such that the photons gain energy (opposite of the Compton effect). This is the most important mechanism responsible for the continuum X-ray emission in accreting HMXBs. The seed photons are produced in the thermal mould of the accretion column (polar caps). For accretion rates typical to HMXBs ($\sim 10^{15-17}$ gm per sec), an asymmetric shock is formed. These photons now have to pass through highly ionized plasma through strong magnetic field of the neutron star across high electron temperature and Thomson optical depth [40]. The photons get up-scattered as they pass through plasma having high energy electrons in strong magnetic fields and produces hard X-rays from a few keV up to several tens of keV.

1.5.2 Characteristic X-rays

In between the continuous X-ray spectrum, we see emission lines visible whenever an excited atom or ion return to lower energy levels by emitting photons. These are the characteristic X-rays produced mostly through flourescense and recombination which

are described below:

Atomic X-ray emission

- Flourescense line emission: X-ray photons above a certain energy are absorbed by atoms/ions via the photoelectric process. This absorption knock off electrons from the innermost orbitals of the atom/ion making it unstable. Thereafter, electrons from higher orbitals take it's place and in the process release a photon with energy equal to the difference of these two orbitals. This is the flourescense line emission.

  In case of X-ray binaries, iron $K\alpha$ line emission play a significant role in probing the density and ionization of matter surrounding the neutron star. Such iron $K\alpha$ lines are produced (in near neutral medium) when electrons from L shell of the atom fill the vacancy in K shell. When electrons from M shell fill the vacancy in K-shell, these give rise to iron $K\beta$ emission lines. When the matter is ionized, and the shielding of the ouer electrons are removed, we see Helium-like and Hydrogen-like iron emission lines (which pertains to emission lines at 6.7 and 6.95 keV). This is seen in a few X-rays binaries like Cen X-3.

- Recombination lines: In the presence of very energetic X-ray photons, the interstellar medium become ionized. When this ion absorbs an electron - recombination emission is produced. The recombination is usually into an excited level. Deexcitation then takes place by the electron cascading down to lower energy levels and in the process giving rise to more emission lines.

1.6 X-ray spectra

HMXBs exhibit a unique type of X-ray energy spectrum characterised by a power-law with photon indices 1-2 and a high energy turnover in the 10-30 keV range. In many cases, an iron $K\alpha$ emission line at ~ 6.4 keV is also observed. Many XRBs also show a soft excess in the low energy part [41, 42]. The high magnetic fields of neutron stars can be directly measured from the cyclotron resonance scattering features (CRSFs). These are seen as absorption features in the X-ray spectrum and are produced due by the scattering of the photons with the electrons quantized into Landau levels in strong magnetic fields. Their centroid energy is related to the NS magnetic field intensity by the equation:

$$E_{\rm C} = 11.6 \frac{B}{10^{12}\,{\rm G}} (1+z)^{-1}\,{\rm keV}, \tag{1.14}$$

where z is the gravitational redshift.

In order to understand the complex physical processes that cause X-ray emission, we need to analyze the X-ray continuum and various emission and absorption lines that modify the continuum. Several attempts have been made to theoretically derive the shape of the X-ray continuum of accreting XRBs [43, 44, 45] but due to the complexity of the physical processes in the accretion column and the magnetosphere, we do not yet have a general model. This is further complicated by the complexity and uncertainity in the geometry of accretion column. The accretion column can be solid or hollow cylinder or may even be of a crescent shape. A new theoretical model based on the bulk and thermal Comptonization occuring in the accreting, shocked gas is one of the most noted contributions made in this field [3]. A schematic view of this model is shown in Figure 1.4. The thermal mould located at the base of the

accretion column through blackbody radiation provide seed photons for upscattering while brehmsstrahlung and cyclotron seed photons arise from the optically thin region above the thermal mound. These photons propagate through a radiation dominated radiative shock medium in the accretion column, undergoing electron scattering, and the observed spectrum is the result of the bulk and thermal Comptonization of these seed photons. The authors reproduced the phase averaged spectra of a few bright sources, Her X-1, Cen X-3 and LMC X-4 using this. On similar lines, another theoretical model 'COMPMAG'[1] - recently proposed [46, 47] - also describes the spectral formation with both thermal and bulk Comptonization processes taken into account (for a few brighter XRBs like Cen X-3, 4U 0115+63, and Her X-1). The main difference between these models being the adaptation of cylindrical geometry for accretion column in the latter. Even though such models describe the X-ray spectra of such chosen XRBs, a unified physical model is still awaited.

In such a scenario, phenomenological models (mentioned in Section 1.10.2) are used to describe the continuum energy spectrum.

The spectrum of XRBs also changes across the pulse phase [48]. In order to specifically study the spectral changes with pulse phase, we need to extract X-ray spectra at specific pulse phases. This is termed as 'Pulse Phase Resolved Spectroscopy' which give us a picture of how the spectrum undergoes periodic changes over each pulse. There are plenty of examples on the use of this technique [49, 50, 51, 52].

[1]https://heasarc.gsfc.nasa.gov/xanadu/xspec/manual/XSmodelCompmag.html

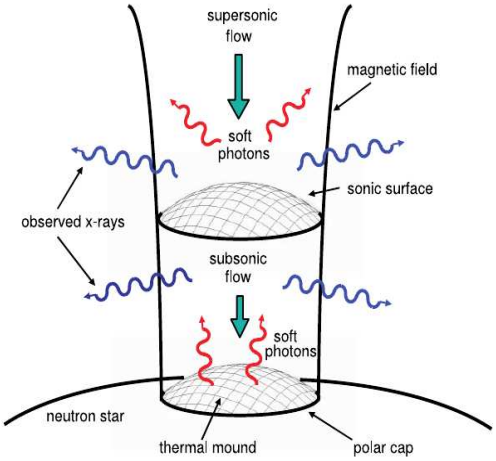

Figure 1.4: An illustration of accretion onto the magnetic polar caps of the neutron star. Seed photons are created throughout the accretion column by bremsstrahlung and cyclotron emission while additional blackbody seed photons are emitted from the thermal mound surface at the base of the column. Figure courtesy: [3].

1.7 Various ways to produce variability in HMXBs

The X-ray lightcurve and spectra of XRBs exhibit a lot of intensity variation. These variability maybe attributed to one of the following cases:

- Be stars: In case of Be stars, there is an increased accretion when the compact object passes through the circumstellar disc of the companion star during peristron passage. This increased accretion leads to Type I outbursts and very high luminosities (10^{37} erg s^{-1}) have been observed. Apart from this, there are also Type II outbursts which cannot be attributed to the orbital passage. Note that there is however another class of persistent Be-XRBs, eg, X-persi; [53], SWJ2000.6+3210; [54] which interestingly do not show Type-I outbursts.

- Roche lobe overflow: The formation of Roche lobe has been described earlier. These are prevalent in most LMXBs in which the orbital separation between the system are smaller compared to HMXBs. In such HMXBs when the companion is filling it's Roche lobe, high accretion rates of 10^{37-38} erg s^{-1} are observed. It can also reach upto 10^{40} erg s^{-1} in Ultra Luminous X-ray Sources (ULXs) [55].

- Supergiant stars: The X-ray variability in case of supergiant systems are for different reasons. The incoming matter from the companion star is channelled along the magnetic field lines of the neutron star which has a strong magnetic field strength of 10^{12} G. The neutron star captures only a fraction of the stellar wind emitted from the companion star [36, 34, 56]. and the gravitational energy of this captured matter is thus released as X-rays.

  The variability in X-rays for such systems, not necessarily correlated to its orbital motion, is because the stellar wind emitted from the companion star is not homogeneous but rather has a clumpy nature. This leads to an increased accretion when the neutron star passes through this dense portion of the wind leading to the simultaneous variability in X-rays.

  The X-ray variability can be well studied by X-ray spectral analysis. The passage of neutron star through a dense wind is characterized by an increase in the hydrogen column density and mostly a simultaneous increase in the equivalent width of Fe $K\alpha$ line if the clumpy matter is present along the line of sight between the source and the observer. Such cases will be ellaborately discussed in Chapters 6 and 7. If a large equivalent width of Fe $K\alpha$ line is not accompanied

with a large column density, it means the reprocessing material (that produces the iron line) is behind the NS as seen in the case of GX 301-2 [57]. On the other hand, changes in accretion rate could be because of the onset of different accretion mechanisms - magnetic or centrifugal gating [39]. Such cases can be identified when there is an increased accretion without a significant change in the hydrogen column density but rather a change in the spectral index like in the case of IGR J16195-4945 [58, 59].

1.8 Pulse profiles

The rate of X-ray photons collected over time is termed as lightcurve. These lightcurves exhibit periodicities corresponding to the spin period of each pulsar. If we fold the light curve with the corresponding pulse period, we get pulse profiles. Pulse profiles describes the variation in the intensity of X-ray photons as the pulsar rotates. The pulse profiles vary greatly in shapes and amplitudes [48, 35, 60] but are unique to each pulsar.

Unlike isolated pulsars, where pulse profiles is determined by the orientation of the spin and magnetic field axes with respect to the observer, viewing angle, NS magnetic field and the gravitational light bending, in case of XRBs, many other factors contribute to make the pulse profile more complex. These include the accretion geometry, radiative transfer taking place in the strongly magnetized plasma, the geometry of the emission region and the mass accretion rate. The pulse profiles appear single peaked, double peaked and in some cases multiply peaked depending upon the visibility of the hotspots [61]. At higher energies above their cyclotron energies, the

pulse profiles look simpler and mostly reflect the intrinsic beaming pattern. Various models have been proposed taking into consideration, the emission regions and the beaming patterns [62, 63] but a general model for pulse profiles is still awaited.

At critical luminosity of $\sim 10^{37}$ erg s^{-1}, the shape of the pulse profile undergo a transition, perhaps due to change in the geometry of the beaming pattern at that luminosity [64]. At luminosities less than the critical value, the gas falls freely down to the neutron star surface and the emitted photons will escape in the direction of the magnetic field, forming a pencil-beam pattern. On the other hand, if the X-ray luminosity is greater than 10^{37} erg s^{-1}, a radiative shock forms at a certain distance above the surface of the neutron star. The emitted photons then get scattered out from the sides of the accretion column to form a fan shaped beam. This is illustrated in Figure 1.5. While low energy pulse profiles are subject to scattering and absorption along the accretion column or by the surrounding matter, the high energy pulse profiles should give a better insight of the beaming pattern.

Pulse profiles for some pulsars are dependent on the luminosity [65]. Some pulsars also exhibit phase reversals of 180 ° in going from lower energy to higher energies [66]. Sudden 'dips' are also seen at certain pulse phases, perhaps due to the eclipse of the emitted radiation by optically thick material in the accretion column [67]. Interestingly, at pulse phases close to the dips, the spectrum varies greatly with large variation in the optical depth which could be due to accretion column being extended only along one direction at these phases [68, 69]. These dips can also be explained by large absorption in that phase [49, 50, 51, 52] which could be due to the accretion stream blocking our line of view at those phases.

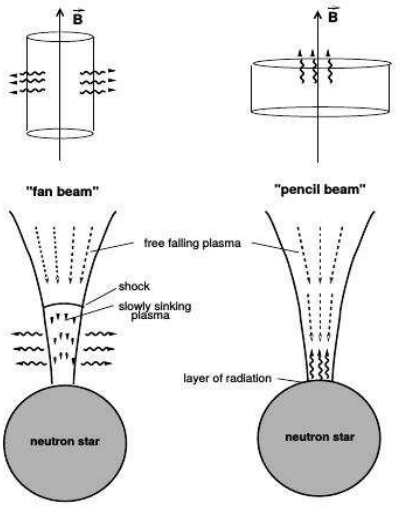

Figure 1.5: Pencil and fan beam emission: At luminosities less than 10^{37} erg s^{-1}, we see pencil beam emission as the emitted photons escape along the magnetic field direction while for luminosities above that the emitted photons get scattered out from the sides of the accretion column to form a fan shaped beam. Figure courtesy: [4].

1.9 Isolated pulsars - a brief discussion

Isolated or rotation powered pulsars (RPPs) as the name implies are rotating neutron stars whose rotation is at the expense of the loss in it's rotational energy. The magnetic field in such pulsars, for simplicity, are assumed to be dipolar. Rapid rotation of these pulsars coupled with strong magnetic fields results in rotation-induced electric field which in turn accelerates the e^+-e^- pairs in the magnetosphere resulting in curvature radiation and leads to high energy (γ-/X-ray) emission either by pair-photon cascades initiated by high energy photons above a polar cap [70, 71, 72] or in the outer gap [73, 74, 75, 76, 77]. The X-ray emission contains thermal and non-thermal components. The thermal emission is further divided into non-pulsed and pulsed components. While the non-pulsed component originates from the cooling of the neutron star surface and of course, is emitted from the whole pulsar with

a characteristic temperature of $\sim$ 0.1 keV, the pulsed component comes from 'hot spots' on the pulsar surface similar to accretion powered pulsars. These 'hot spots' are heated by the bombardment of relativistic particles that come from the pulsar magnetosphere [78, 79, 80]. Non thermal emission arises from charged relativistic particles accelerated in the pulsar magnetosphere, and it might also contain pulsed [81, 82] and non-pulsed components [83, 84]. In some cases, a pulsar wind nebula (PWN) is found to surround a RPP. The X-ray emission of the PWN is non-pulsed and often dominates the non-thermal emission of the system.

1.10 Tools used in analysis

1.10.1 Timing analysis tools

Timing analysis for *Suzaku*, *RXTE* and *Swift* are performed with a general purpose timing analysis package `XRONOS` which comes embedded with `FTOOLS`. It includes programs for generating light curves, power spectrum, epoch folding, auto and cross correlation and various other statistical techniques. Given below are a brief description of the timing analysis tools used in this thesis.

- `lcurve`: This program produces binned lightcurves from input file. It can plot up to four simultaneous energy time series at once. For multiple simultaneous light curves, it can also plot the hardness ratio of the lightcurves and their sum.

- `efsearch`: The lightcurve can be fed to this tool which then searches for period-

icities in it by folding data over a trial period range which we specify, determines the χ^2 of the folded lightcurve when fitted to a constant, plots the χ^2 values versus the trial periods and output the results in a FITS file format.

- `efold`: This tool is used for folding light curves with a periodicity that we give as input with respect to an epoch. It calculates folded lightcurves, plots and outputs the results.

- `powspec`: This tool produces a power spectral density for one time series, plots and outputs the results in a FITS file. It also takes the lightcurve as it's input.

1.10.2 Spectral analysis tools

The X-ray spectrum that we obtain from the detector is not the actual source spectrum, but rather photon counts (C) within specific instrument channels, (I). This observed spectrum is related to the actual spectrum of the source $f(E)$ by:

$$C(I) = \int_0^\infty f(E)R(I,E)dE \tag{1.15}$$

where R(I,E) is the instrumental response for the particular detector and is proportional to the probability that an incoming photon of energy 'E' will be detected in channel 'I'. At first look, it appears straightforward and it seems that we could easily invert the equation to obtain the source spectrum $f(E)$. This, however, is not possible as such inversions are non-unique and unstable[2].

The alternative then is to choose a model spectrum $f(E)$ that can be described by few parameters and then fit to the data measured by the spectrometer. For each

[2]http://heasarc.gsfc.nasa.gov/xanadu/xspec/manual/XspecSpectralFitting.html

$f(E)$, a predicted count spectrum is calculated and compared to the observed data $C_{obs}(I)$. A fit statistics is then computed to obtain the goodness of the fit. The fit statistics we have used is the χ^2 which is defined as:

$$\chi^2 = \sum (C(I) - C_{obs}(I))^2/(\sigma(I))^2 \tag{1.16}$$

where $\sigma(I)$ is the error associated with each count C(I). The χ^2 is estimated for a certain number of degrees of freedom ν given by number of channels minus the number of model parameters. In general a fit is said to be satisfactory if the reduced; χ^2_{red} (χ/ν) is ~ 1. A χ^2_{red} that is much greater than one indicates a poor fit, while a χ^2_{red} that is much less than one indicates that the errors on the data have been over estimated or the model has been over specified, like too many parameters than what can be measured with the given data. The confidence interval or the error associated with a given parameter is computed by varying the parameter value until the χ^2 increases by a particular number above the best-fit value. The analytical form of the four empirical spectral models considered in this thesis are:

$$\text{HIGHECUT}(E) = A\ E^{-\Gamma} \times \begin{cases} 1 & (E \leq E_{\text{cut}}\ ) \\ \mathrm{e}^{-(E-E_{\text{cut}}\ )/E_{\text{fold}}} & (E > E_{\text{cut}}\ ) \end{cases} \tag{1.17}$$

(where Γ is the photon index, E_{cut} the cutoff energy, and E_{fold} the folding energy),

$$\text{NPEX}(E) = A(E^{-\Gamma_1} + BE^{+\Gamma_2})\mathrm{e}^{-E/E_{\text{fold}}} \tag{1.18}$$

(where Γ_1 and Γ_2 are the photon indices with positive values - Γ_1 was frozen to 2.0, and E_{fold} the folding energy),

$$\mathrm{FDCUT}(E) = A\ E^{-\Gamma}\ \frac{1}{1+\mathrm{e}^{(E-E_{\mathrm{cut}}\ )/E_{\mathrm{fold}}}} \tag{1.19}$$

(where Γ is the photon index, E_{cut} the cutoff energy, and E_{fold} the folding energy), and

$$\mathrm{NEWHCUT}(E) = \begin{cases} E^{-\Gamma} & E \leq E_{\mathrm{cut}}\ - W/2 \\ AE^3 + BE^2 + CE + D, & E_{\mathrm{cut}}\ - W/2 \leq E \leq E_{\mathrm{cut}}\ + W/2 \\ E^{-\Gamma} \times\ \mathrm{e}^{(E_{\mathrm{cut}}\ -E)/E_{\mathrm{fold}}}, & E \geq E_{\mathrm{cut}}\ + W/2 \end{cases} \tag{1.20}$$

(where Γ is the photon index, E_{cut} the cutoff energy, E_{fold} the folding energy, and W is the width used to smoothen the abrupt break in HIGHECUT at E_{cut}).